Progress In Electromagnetics Research, Vol. 122, 77–92, 2012

COMPACT HYBRID COAXIAL ARCHITECTURE FOR 3–10 GHz UWB QUASI-OPTICAL POWER COMBINERS

I. Russo[1,*], L. Boccia[2], G. Amendola[2], and H. Schumacher[3]

[1]Institut für Mikrowellentechnik, Universität Ulm, Ulm 89081, Germany

[2]Dipartimento di Elettronica, Informatica e Sistemistica, Università della Calabria, 87036 Rende (CS), Italy

[3]Institut für Elektronische Bauelemente und Schaltungen, Universität Ulm, Ulm 89081, Germany

Abstract—Tray-type quasi-optical (QO) power combiners are able to combine the high- and medium-output power of QO systems with the well-known advantages of pulsed ultra-wideband (UWB) systems. In this work, an alternative low-profile tray-type passive structure for 3 GHz–10 GHz power combining is proposed. The purpose of the proposed solution is to reduce the physical size with respect to other existing architectures by using hybrid coaxial lines. In spite of the reduced size, the structure maintains ultra-wideband operation and high combining efficiency, as proved through measurements. Therefore, the proposed structure is suitable for integration with monolithic microwave integrated circuit (MMIC) amplifiers for medium- and high-power generation, depending on the type of MMICs which are integrated into the passive combiner. Numerical analyses of the designed power combiner integrated with some MMIC amplifiers reveal its benefits in terms of increased output power and wider dynamic range compared to isolated MMICs.

1. INTRODUCTION

A rapid diffusion of ultra-wideband (UWB) technologies into the military and civil markets has been observed in recent years. The main reasons can be attributed to the numerous advantages that UWB offers in comparison to narrowband systems. The power

Received 17 October 2011, Accepted 8 November 2011, Scheduled 14 November 2011

* Corresponding author: Ivan Russo (ivan.russo@uni-ulm.de).

spectral density of UWB signals is extremely low, enabling UWB systems to operate in the same spectrum as narrowband technologies without causing undue interferences. Examples of UWB techniques can be found in medical monitoring and imaging [1–3], high-data rate communication systems [4], high precision Radars for tracking and positioning applications and radio frequency identification (RFID) [5], Ground Penetrating Radars (GPR) [6] and analysis of biological tissues with high-absorption. The generation of millions of UWB pulses per second allows the deep penetration of a wide range of materials such as building blocks, plastic and wood.

Nevertheless, UWB frontends also need sources generating power levels that are able to penetrate high-absorption materials. Single solid-state amplifiers are often unable to provide the power level needed in such applications. Quasi-optical (QO) or spatial power combining systems [7] have shown, in the last two decades, their promising capabilities to produce medium- and high-output power levels for frequencies spanning from the microwave to millimeter-wave ranges. The key concept of a QO combiner is the use of a high-efficient combining network containing several active sources. A QO power combiner consists of a number of solid-state devices, each of them equipped with a transmitting and a receiving antenna. The use of free-space networks for the distribution of the input signal and for the re-combination of the amplified contributions permits a strong reduction in terms of losses in comparison to conventional folded combiners. The main reason for this is that the power combining process takes place in the surrounding air.

The attention of researchers in the field of QO combiners has been particularly focused on tile-type grid amplifiers [8–10], amplifier arrays [11–14] and oscillators [15, 16]. Referring to the tile-type family, represented by grid amplifiers and amplifier arrays (Figure 1(a)), the operating principle is based on the amplification of a free-space wave coming from an external source. A y-polarized incident wave excites RF currents on the receiving antennas of the array/grid, each of which is connected to an amplifier. The amplified versions of those currents are then radiated to the output with 90°-rotated polarization and the single phase-coherent contributions sum up in the free-space to form a high-power output signal. Due to the omni-directional nature of the antennas employed in this kind of structures, the input/output (I/O) isolation must be realized by means of two orthogonal polarizers positioned at the two extremes of the system. The resulting resonant cavity has a positive impact on the gain and on the I/O isolation but limits the applicability of the technique to narrowband systems.

If the polarizer-cavity is removed and UWB end-fire radiators,

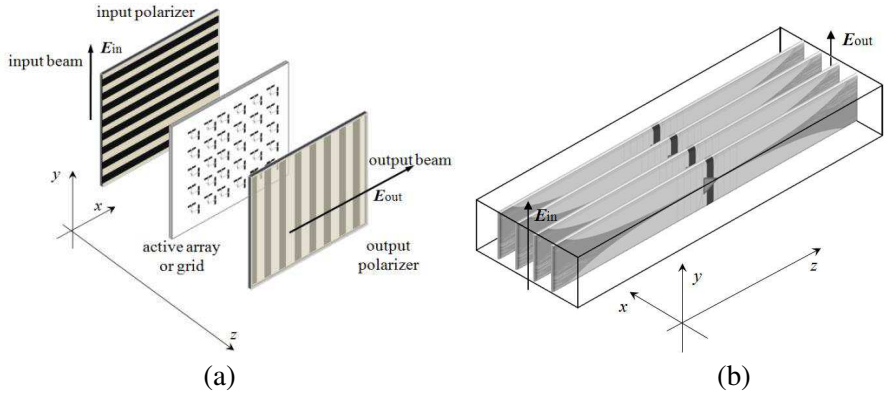

Figure 1. QO power combiners. (a) Tile-type. (b) Tray-type.

such as Vivaldi [17] or Quasi-Yagi [18] antennas, are used in place of dipoles or slots, the bandwidth of the power combiner can be increased. Moreover, several layers or "trays" can be stacked to form an array as shown in Figure 1(b). This configuration defines the second family of QO power combiners, namely the "tray-type" family. The UWB properties depend not only on the antennas, but also on the amplifiers and on the surrounding environment. The amplifiers must offer UWB properties in terms of flat gain and low distortion. The surrounding environment must contain the tray array to avoid that the input power partially overcomes the effective input section of the combiner, which results in the so called "spillover losses". For this reason, the trays are inserted into a closed propagation environment, such as a rectangular waveguide. A combining technique using finline arrays in a rectangular waveguide, shown in Figure 1(a), was described in [19]. In this approach, finline transitions couple the energy from the waveguide field to a set of MMIC amplifiers. The architecture proposed in [19] used a 24-MMIC system and produced over 120-W continuous wave (CW) power in the waveguide environment. This system showed a relatively narrow bandwidth, since the operating frequency range is defined by the propagation of the sole TE_{10} mode. Moreover, using a rectangular waveguide the different finlines are not uniformly driven in amplitude. Another problem is that the dispersive characteristics of the rectangular waveguide cause distortion issues when dealing with amplification of pulses. Those difficulties can be overcome by re-adapting the approach to a TEM wave-guiding environment, such as a circular coaxial waveguide. This might be done by distributing tapered finline structures in the annular aperture of an oversized round coaxial

line. Such a structure can accommodate a large number of active trays, provide uniform illumination of the array, and can be designed for ultra-wideband operation. This concept was first introduced in [20] and subsequently used in [21] to design a 2 GHz-to-16 GHz combiner with a 75% combining efficiency and 30 dBm output power using 64 MMIC amplifiers on 32 trays, at the expense of a relatively large size.

In this work, a hybrid rectangular coaxial line is demonstrated as a passive combining environment for UWB QO amplifiers. This solution, even though it reduces the active device integration density, is more suitable to realize low-profile medium-power structures than a bulky full-3D round architecture.

2. UWB TRAY-TYPE QO POWER COMBINER ARCHITECTURE

The proposed 3 GHz-to-10 GHz power combiner, shown in Figure 2, is based on a TEM waveguide where two ultra-wideband exponentially-tapered finlines are used to couple the quasi-TEM mode propagating in the rectangular quasi-planar or hybrid coaxial line to the input ports of two amplifier chips. The amplified signals will be then re-transmitted to the output of the combiner using two other symmetric UWB exponentially-tapered finlines.

The hybrid coaxial line is composed of a rectangular metallic package that contains a sandwiched high-permittivity dielectric substrate (Figure 2(b)). Vivaldi-like finline transitions are printed on this substrate. To implement the sidewalls and the center conductor of the coaxial line, a defined number rows of gold plated via-holes are

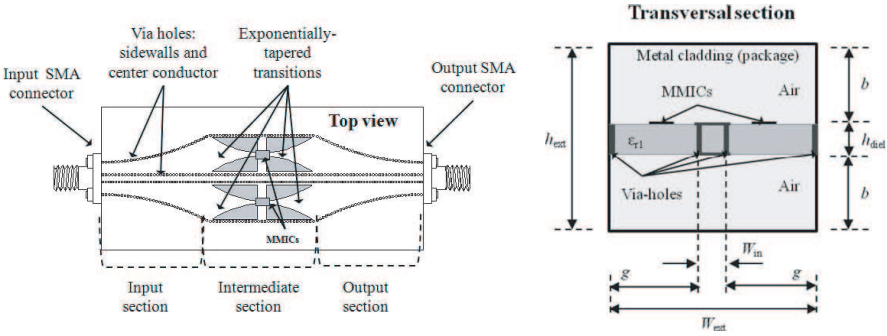

Figure 2. UWB hybrid coax line combiner. (a) Top view. (b) Transversal section.

drilled into the substrate as shown in Figures 2(a) and 2(b). The fact that the structure is partially manufactured using a substrate integrated approach [22, 23] explains the term "hybrid". This concept can be naturally extended from the 1-layer proof-of-concept case, discussed in this work, to an N-layer stack to integrate more devices.

3. DESIGN PROCEDURE

The complete system and all of its sub-parts have been designed to operate in the frequency range between 3 GHz and 10 GHz, namely across a 108%-wide relative bandwidth around a center frequency of 6.5 GHz. The combiner can be divided, for simplicity of synthesis, in several sub-sections to be designed independently, as illustrated in Figure 2(a). The input and output sections of the coaxial line must be interfaced with some 50 Ω SMA connectors. Therefore, those sections must be optimized for a 50 Ω Ohm characteristic impedance. The intermediate section, that contains exponentially-tapered finlines to be connected to the active devices, must be designed to guarantee the propagation of the sole TEM mode. The excitation of TE_{11} degenerate modes must be delayed after the designated upper limit of 10 GHz. Furthermore, the power undelivered to the amplifiers (spillover losses) must be minimized. Finally, Vivaldi-like finline transitions must be designed to ensure a good matching between the theoretical 50 Ω MMIC input/output impedances and the coaxial line characteristic impedance.

3.1. Design of the Empty Hybrid Coaxial Line

The hybrid coaxial line is a rectangular coaxial waveguide formed by two sections: a metal package and a sandwiched dielectric layer. It is, in short, the non-uniform version of the conventional rectangular coaxial line, also called "rectax" [24].

Through full-wave optimizations [25], the transversal dimensions of the intermediate and the 50 Ω sections, as well as the relative permittivity of the dielectric layer, can be determined. At first, the design is carried out by replacing the via-hole walls with continuous metal walls. An important aspect to point out is that the characteristics of the dielectric substrate must be chosen as a trade-off between low spillover losses and inhibition of unwanted modes in the operating range of 3 GHz–10 GHz. Increasing the relative permittivity ε_{r1} and the dielectric thickness h_{diel}, the energy concentration in the central layer of the structure is increased, thereby improving the combining efficiency and reducing the spillover losses. On the other

hand, if the values of ε_{r1} and h_{diel} are too high, the cut-off frequency of the first occurring higher-order mode is anticipated, hence reducing the operating frequency range of the structure.

Referring to Figure 2(b), the optimized values of the intermediate and 50 Ω section of the combiner are listed in Table 1.

Table 1. Geometrical and electrical parameters of the intermediate and 50 Ω sections.

Internal conductor width $W_{\text{in, int}}$ [mm]	2 mm
External conductor width $W_{\text{ext, int}}$ [mm]	12 mm
External conductor height $h_{\text{ext, int}}$ [mm]	7.5 mm
Internal conductor width $W_{\text{in,50}}$ [mm]	2 mm
External conductor width $W_{\text{ext,50}}$ [mm]	7 mm
External conductor height $h_{\text{ext,50}}$ [mm]	4.5 mm
Substrate thickness h_{diel} [mm]	0.762 mm
Substrate relative permittivity ε_{r1}	9.8

The values reported in Table 1 are obtained from a full-wave optimization process to find the best tradeoff between high power concentration in the proximity of the dielectric substrate (to reduce spillover losses) and delayed excitation of higher-order modes. Using the given geometrical and electrical values, the TEM-mode characteristic impedance of the intermediate section is set to 75 Ω. After the dimensions and dielectric characteristics have been chosen, the via-holes used for the inner conductor and sidewalls of the coaxial line must be optimized to avoid lateral losses and to guarantee the necessary TEM boundary conditions for the real configuration. Referring to the equations for substrate integrated waveguides (SIWs) reported in [22] and being $f_{\max}$ the upper operating frequency and $\lambda_{g\_f_{\max}}$ the related wavelength, the hole diameter D and the inter-distance between adjacent holes b can be chosen using (1):

$$\begin{aligned} D &< \lambda_{g\_f_{\max}}/5 \\ b &\leq 2D \end{aligned} \tag{1}$$

Referring to technological limits and to conditions (1), the via-hole diameter is chosen to be $D = 0.4$ mm and the longitudinal inter-distance is set to $b = 0.6$ mm. The via-hole sidewalls and the

internal conductor are then covered on the upper and lower surfaces of the substrate with some metal laminations that extend along the longitudinal direction of the coaxial waveguide. These laminations guarantee the boundary conditions for the E-field at the upper and lower faces of the center conductor and avoid that a portion of the signal travels between the two central rows of via-holes.

Full-wave simulations [25] of the intermediate sections across the frequency range 3 GHz–10 GHz show that the propagation coefficient of the higher order modes ranges between −18 dB and −10 dB for the TE_{11a} mode and between −30 dB and −12 dB for the TE_{11b} mode.

The last step of the design process of the empty hybrid coaxial line is the design of the transition between the 50 Ω and the 75 Ω coaxial sections. The via-hole displacement and the walls of the metal case must be tapered in order to obtain a matching in the 3 GHz–10 GHz range. For simplicity, two linear tapers of an optimized length equal to $l_t = 25$ mm are used to interface the input and output sections with the intermediate section of the hybrid line. A sketch of the empty hybrid coaxial line is depicted in Figures 3(a) and 3(b). Full-wave simulations of the complete empty coaxial structure provide the reflection and transmission coefficients in Figure 3(c), proving the good performances of the hybrid TEM line in the range of 3 GHz–10 GHz. The transmission S-parameter, S_{21}, is very close to 0 dB across the

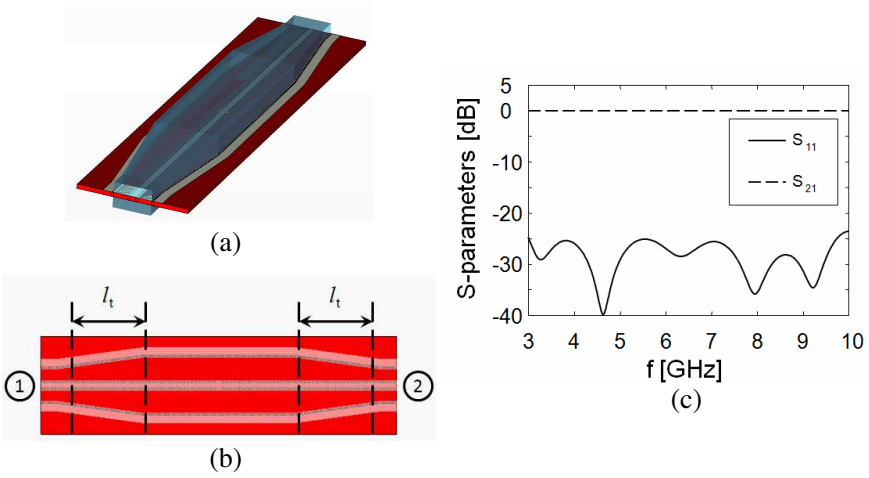

Figure 3. (a) Empty coaxial combiner model [25]. (b) Top view: the linear tapers between the 50 Ω and the intermediate sections are 25 mm long. (c) Simulated S_{11} and S_{21} of the designed empty hybrid coaxial line structure.

whole range and the reflection coefficient at the input port, S_{11}, is always maintained below -25 dB.

3.2. Design of the Exponentially-tapered Finline Transition

In order to couple the energy travelling inside the hybrid coaxial structure to the internal MMICs, some UWB matched transitions need to be designed. Those transitions are defined in literature as "antennas", but they are nothing but finlines inserted into the waveguide environment. The Vivaldi-like shape is able to provide a considerable wide band and a relatively low group delay. In this work, exponentially-tapered finline transitions are used.

The matching problem using an exponential taper is illustrated in Figure 4(a). The impedance called Z_{MMIC}, assumed to be $50\,\Omega$, must be matched to the impedance Z_{LOAD}, which is the impedance of the coaxial line seen by the single taper. The value of Z_{LOAD} is different from the characteristic impedance Z_{TEM} of the structure. Because of mode symmetry considerations, given N active devices and, consequently, N exponential tapers, the impedance seen at the end of every single tapered line is N times Z_{TEM}. For the case at hand, $Z_{\mathrm{LOAD}} = 2Z_{\mathrm{TEM}} = 150\,\Omega$, as illustrated in Figure 4(b).

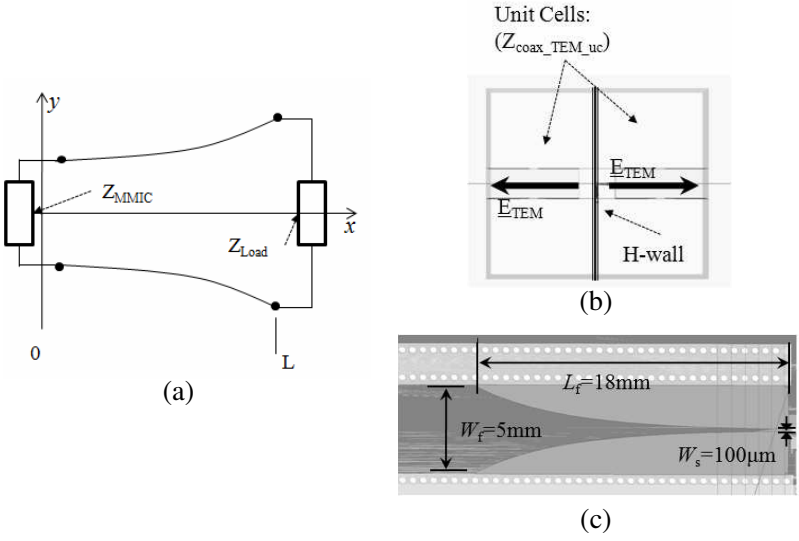

Figure 4. (a) Matching using exponentially-tapered finlines. (b) Impedance multiplication due to even mode symmetry. (c) Optimized finline transition.

The equations given in [26] for the synthesis of Vivaldi antennas can be used for a preliminary estimation of the taper parameters and are reported in (2) and (3):

$$y = c_1 e^{ax} + c_2 \tag{2}$$

$$c_1 = \frac{y_1 - y_2}{1 - e^{aL}}, \quad c_1 = \frac{y_2 - y_1 e^{aL}}{1 - e^{aL}} \tag{3}$$

where L is the taper length and a is the exponential coefficient defined in (4):

$$a = \frac{1}{L} \ln \left(\frac{Z_{\text{LOAD}}}{Z_{\text{MMIC}}} \right) \tag{4}$$

A further full-wave optimization needs to be performed in order to improve the matching of the single finline to the intermediate section of the hybrid coaxial waveguide. Figure 4(c) shows the single finline with optimized parameters. For technological reasons, the width of the terminating slotline where the amplifier chips must be connected is chosen to be $W_s = 100\,\mu\text{m}$. The entire taper is $L_f = 18\,\text{mm}$ long and has a maximum aperture $W_f = 5\,\text{mm}$. The exponential coefficient in (2) is afterwards optimized to a final value of $a = 0.2$. The two transitions at the input, as well as the two towards the output, are printed on opposite sides of the substrate to guarantee a complete axial symmetry to the structure. The sketch of the complete passive combiner is shown in Figure 5(a).

A full-wave simulation of the electromagnetic field propagating in the structure proves the correct design of the UWB power combiner based on hybrid coaxial lines and exponential finlines. In the simulation, the input and output finlines are terminated with $50\,\Omega$ ports. As it is shown in Figure 5(b), the highest amount of travelling

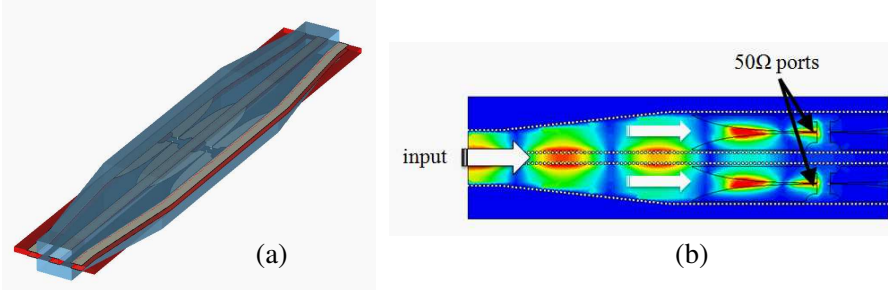

Figure 5. (a) Complete passive UWB combiner model [25]. (b) Full-wave simulation of the input electric field absorbed by the $50\,\Omega$ loads at the finline terminations [25].

power is transferred to the internal 50 Ω ports. As a consequence, very low spillover losses are expected. Furthermore, it can be noticed that there is no loss of power through the sidewalls, proving the correct design of via-hole metallizations. In the next section, a comparison between measured and simulated S-parameters of the passive UWB combiner will be discussed. From the measured scattering parameters, the power combining efficiency of the passive device will be extracted.

4. EXPERIMENTAL PERFORMANCES OF THE PASSIVE COMBINER

The passive UWB power combiner is subsequently manufactured and experimentally tested. The measured S-parameters are then compared to the simulated ones to demonstrate the validity of the simulation model as well as testing the performances of the fabricated device. The sandwiched substrate is ARLON 1000 laminate with $\varepsilon_r = 9.8$. The building blocks forming the hybrid coaxial line can be simply stacked and tightened up, as illustrated in Figures 6(a) and 6(b), where the fabricated prototype is shown. The final transversal dimensions of the device (comprehensive of external metal case) are 2×3 cm. The total length, including input and output SMA connectors, is equal to 11 cm.

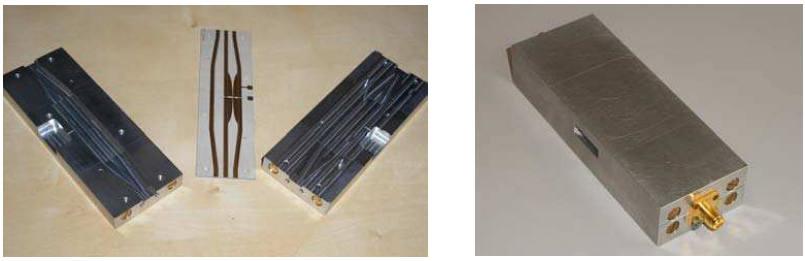

(a) (b)

Figure 6. (a) Building blocks of the manufactured passive combiner. (b) Assembled prototype: the upper and lower metal halves and the substrate are stacked together.

To correctly measure the spillover losses of the passive UWB combiner, four 50 Ω chip resistors are connected to the internal terminations of the two input and two output finlines, as shown in Figure 7. This is done in order to emulate the port impedances of internally-matched MMIC amplifiers. The same arrangement

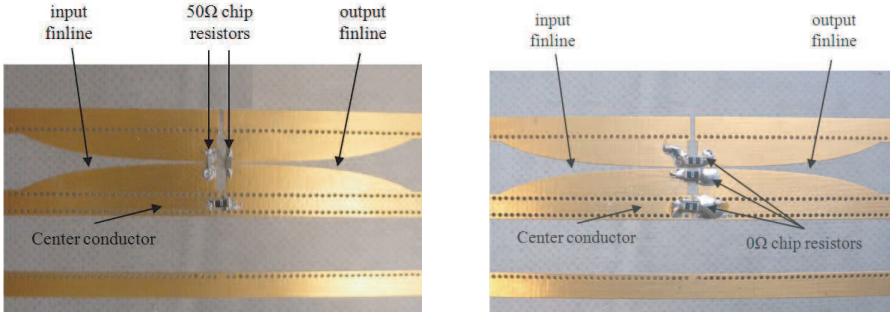

(a) (b)

Figure 7. Input and output finlines set for the measurement of the passive combiner. (a) Spillover measurement: 50 Ω chip resistors are soldered at the finline terminations to emulate the I/O impedances of a broadband-matched MMIC amplifier. (b) Back-to-back measurement: input and output transitions are shorted using of two 0 Ω chip resistors.

is symmetrically repeated on the opposite face of the substrate. Furthermore, Figure 7(a) shows a 0 Ω series resistor that is only used during the passive combiner measurement in place of a chip capacitor to short the cut in the center conductor. This cut has been predisposed to prevent the formation of any DC feedback current through the center conductor in the active configuration. Those currents could negatively affect the stability of the active device and must be blocked by means of an open circuit. On the other hand, to guarantee a correct RF behavior and avoid discontinuities in the field distribution, the active configuration will require that a series chip capacitor is soldered on the left part of the center conductor and bonded to the right part (in place of the 0 Ω chip resistor only used during the passive test). Doing so, the cut in the center conductor will be seen as a short circuit at RF, without affecting the TEM mode distribution at the center of the structure. The spillover losses are defined, for the test of the passive combiner, as the energy which is not delivered to the internal 50 Ω chip resistors connected to the input finlines. This energy overcomes the intermediate combining section and travels to the output port of the coaxial line, being unusable for power combining purposes. In the case at hand, those losses can be evaluated by measuring the S_{21_SL} between the input and the output connectors of the hybrid coaxial line with passive loads. The S-parameters S_{11} and S_{21_SL} obtained from the full-wave simulation and measurement for the passive combiner are reported in Figure 8(a). The measured results are

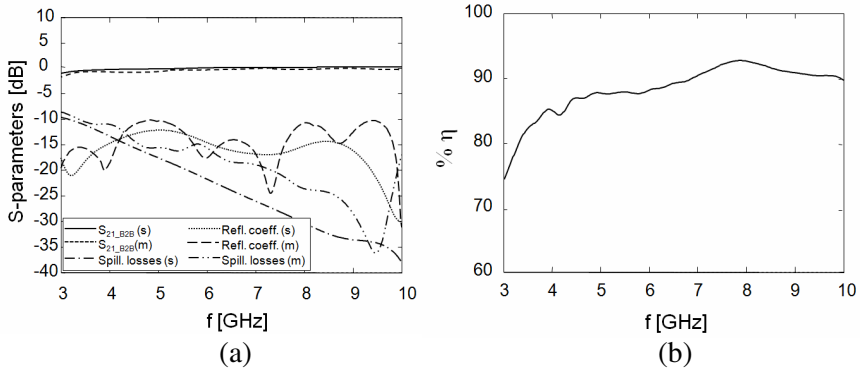

Figure 8. (a) Simulated (s) and measured (m) S-parameters of the UWB power combiner. (b) Measured power combining efficiency.

in good agreement with simulated ones, showing good performances of the passive combiner. The reflection coefficient at the combiner input is kept below $-10\,\mathrm{dB}$ across the whole operating range. As shown in Figure 8(a), the measured spillover losses are very low and their values range from $-10\,\mathrm{dB}$ to $-35\,\mathrm{dB}$ in the operating frequency interval. This result is in good agreement with the simulated field pattern shown in Figure 5(b). However, the spillover losses at low frequencies are slightly worse than what is observed at higher frequencies. This is the consequence of the frequency-dependent amplitude distribution of the travelling power: as the frequency increases, more power tends to concentrate close to the substrate and it is better coupled to the internal ports through the tapered transitions.

The effective power which is absorbed by the internal $50\,\Omega$ input ports and that can be delivered towards the output can be determined by a back-to-back measurement of the combiner. To measure the back-to-back $S_{21\_B2B\_TOT}$ total transmission, all the internal $50\,\Omega$ loads are removed and the input and output exponentially-tapered transitions are directly connected to each other through $0\,\Omega$ chip resistors (Figure 7(b)). The effective back-to-back transmission coefficient S_{21_B2B} between input and output connectors is obtained by depurating measured $S_{21\_B2B\_TOT}$ from the spillover losses S_{21_SL}, measured using the setup with the $50\,\Omega$ chip resistor loads. The measured back-to-back transmission S_{21_B2B} includes conductor and dielectric losses of the hybrid combiner and it is in good agreement with the simulated one, as described in Figure 8(a).

The total power combining efficiency of the passive combiner can

be defined through the formalism in (5):

$$\%\eta = \frac{\sum_{k=1}^{N} P_{o,k}}{P_i} \cdot 100 \tag{5}$$

where N is the maximum number of internal unit cells (number input-output finline pairs), P_i is the total amount of power delivered to the input connector of the power combiner and $P_{o,k}$ is the power contribution at the output connector from the k-th unit cell in the measured passive configuration. The combining efficiency quantifies the capability of the combiner to absorb and distribute the incoming energy to each of the N internal input ports and to recombine the N re-transmitted contributions to the output connector of the structure. The combining efficiency of the designed passive combiner can be extracted by combining the scattering parameters of the two previously described passive measurement setups and it exhibits values between 74% and 92%, as shown in Figure 8(b). The slightly worse spillover losses at low frequencies determine the drop in efficiency to 74%.

5. STUDY OF THE INTEGRATION WITH SOLID-STATE DEVICES

The integration of the designed passive combiner with MMIC amplifiers is tested through some circuit simulations performed in [27]. The measured scattering matrix of the hybrid coaxial combiner is imported into the simulation environment and connected to the non-linear models of a pair of MMIC amplifiers. Between 3 GHz and 10 GHz, the MMIC model exhibits a flat gain around 25 dB and input and output reflection coefficients below −10 dB. Figure 9(a) illustrates the simulated S-parameters of the active power combiner with two

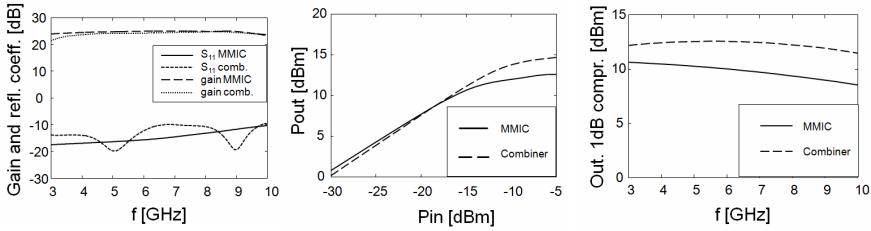

Figure 9. Simulation of the measured scattering matrix of the hybrid passive combiner with UWB MMICs vs MMICs: (a) Gains and reflection coefficients. (b) Input and output power at 6.5 GHz. (c) Output 1 dB compression point vs frequency.

integrated MMICs in small signal conditions. In complete agreement with the theory, the QO power combiner shows a gain that is almost overlapping with the one of the single MMIC and it exhibits good input and output matching across the whole frequency range. Further simulations show that the stability criterion is also fully accomplished.

The large signal analysis of the MMIC and the combiner demonstrates that the spatial combining is able to increase the maximum linear output power because the input and output dynamic ranges are improved by a factor of N, where N is the number of devices integrated in the system. This effect can be explained as a shift towards higher input power levels of the 1 dB compression point. In the case at hand, the dynamic ranges are doubled, where $N = 2$. This phenomenon can be observed in Figure 9(b), where the output power versus input power for the MMIC and the active combiner are plotted at the center frequency of 6.5 GHz. The output 1 dB compression point vs. frequency of both MMIC and active combiner is reported in Figure 9(c), demonstrating the improved (doubled) linearity over the operating frequency range. The higher spillover loss at 3 GHz determines a smaller improvement of the output dynamic range with respect to higher frequencies, namely 2.3 dB instead of 3 dB.

6. CONCLUSIONS

The design of UWB power combiners requires the adoption of a tray-type scheme combined with a coaxial wave-guiding environment. The passive architecture proposed in this work uses a hybrid coaxial line integrated with Vivaldi-like finline tapers to realize a compact power combiner operating from 3 GHz to 10 GHz. The idea is to combine partially substrate integrated coaxial lines with an external metal package in order to reduce the transversal size of the device. Besides the reduced dimensions, the proposed structure is also cost-effective and easily mountable, due to its stack-scheme. Simulations and measurements of the proposed combiner, based on two-finline input/output sections, shows very good impedance matching properties and very high power combining efficiency across the entire frequency interval spanning from 3 GHz to 10 GHz. Further analyses of the active configuration of the designed power combiner demonstrate its capabilities to double the linear dynamic range and increase the maximum output power with respect to the isolated integrated MMICs. It is possible to increase the linearity-widening effect by extending the proof-of-concept two-MMIC scheme, described in this work, to an N-MMIC configuration that employs several stacked finline layers.

REFERENCES

1. AlShehri, S. A., S. Khatun, A. B. Jantan, R. S. A. Raja Abdullah, R. Mahmood, and Z. Awang, "Experimental breast tumor detection using Nn-based UWB imaging," *Progress In Electromagnetics Research*, Vol. 111, 447–465, 2011.
2. Lazaro, A., D. Girbau, and R. Villarino, "Analysis of vital signs monitoring using an IR-UWB radar," *Progress In Electromagnetics Research*, Vol. 100, 265–284, 2010.
3. AlShehri, S. A., S. Khatun, A. B. Jantan, R. S. A. Raja Abdullah, R. Mahmood, and Z. Awang, "3D experimental detection and discrimination of malignant and benign breast tumor using Nn-based UWB imaging," *Progress In Electromagnetics Research*, Vol. 116, 221–237, 2011.
4. Fullerton, L. W., "Spread spectrum radio transmission system," US Patent 4,641,317, 1987.
5. McEwan, T. E., "Ultra-wideband radar motion sensor," US Patent 5,361,070, 1994.
6. Daniels, D. J. and I. O. E. Engineers, *Ground Penetrating Radar*, IET, 2004.
7. Mink, J. W., "Quasi-optical power combining of solid state millimeter-wave sources," *IEEE Trans. Microw. Theory Tech.*, Vol. 34, 273–279, 1986.
8. Kim, M., et al., "A grid amplifier," *IEEE Microw. Guided Wave Lett.*, Vol. 1, 322–324, 1991.
9. Cheung, C. T., M. P. De Lisio, J. J. Rosenberg, R. Tsai, R. Kagiwada, and D. B. Rutledge, "A single chip two-stage W-band grid amplifier," *IEEE MTT-S Int. Microw. Symp. Dig.*, Vol. 1, 79–82, 2004.
10. Russo, I., L. Boccia, G. Amendola, G. Di Massa, and P. S. Hall, "Simple model for the parametric analysis of grid amplifiers," *IET Microw., Ant. Prop.*, Vol. 3, No. 5, 877–881, Aug. 2009.
11. Tsai, H. S., M. J. W. Rodwell, and R. A. York, "Planar amplifier array with improved bandwidth using folded slots," *IEEE Microw. Guided Wave Lett.*, Vol. 4, 112–114, 1994.
12. Marshall, T., M. Forman, and Z. Popovic, "Two Ka-band quasi-optical amplifier arrays," *IEEE Trans. Microw. Theory Tech.*, Vol. 47, 2568–2573, 1999.
13. Ortiz, S. C., J. Hubert, L. Mirth, E. Schlecht, and A. Mortazawi, "A high-power Ka-band quasi-optical amplifier array," *IEEE Trans. Microw. Theory Tech.*, Vol. 50, 487–494, 2002.

14. Russo, I., L. Boccia, G. Amendola, and G. Di Massa, "Simplified design flow of quasi-optical slot amplifiers," *Progress In Electromagnetics Research*, Vol. 96, 347–359, 2009.
15. Bundy, S. C. and Z. B. Popovic, "A generalized analysis for grid oscillator design," *IEEE Trans. Microw. Theory Tech.*, Vol. 42, 2486–2491, 1994.
16. Deckman, B., D. Rutledge, J. J. Rosenberg, E. Sovero, and D. S. Deakin, Jr., "A 1 watt 38 GHz monolithic grid oscillator," *IEEE MTT-S Int. Microw. Symp. Dig.*, Vol. 3, 1843–1845, 2001.
17. Zhang, G., H. Zhang, Z. Wang, and Z. Yuan, "Improvements in a 4-elements high gain directional UWB antenna array," *J. Electromagn. Waves and Appl.*, Vol. 24, No. 4, 453–461, 2010.
18. Song, H., M. Bialkowski, and P. Kabacik, "Parameter study of a broadband uniplanar quasi-Yagi antenna," *13th Int. Conf. Microw., Radar Wireless Commun., MIKON*, Vol. 1, 166–169, 2000.
19. Cheng, N.-S., P. Jia, D. B. Rensch, and R. A. York, "A 120-watt X-band spatially combined solid-state amplifier," *IEEE Trans. Microw. Theory Tech.*, Vol. 47, 2557–2561, Dec. 1999.
20. Alexanian, A. and R. A. York, "Broadband waveguide-based spatial combiner," *IEEE MTT-S Int. Microw. Symp. Dig.*, Vol. 3, 1139–1142, 1997.
21. Jia, P., L. Y. Chen, A. Alexanian, and R. York, "Multioctave spatial power combining in oversized coaxial waveguide," *IEEE Trans. Microw. Theory Tech.*, Vol. 50, 1355–1360, 2002.
22. Wu, K., D. Deslandes, and Y. Cassivi, "The substrate integrated circuits — a new concept for high-frequency electronics and optoelectronics," *6th Int. Conf. Telecommun. Modern Satell., Cable Broadcast. Service, TELSIKS*, Vol. 1, P-III-P-X, 2003.
23. Hu, G., C.-J. Liu, L. Yan, K.-M. Huang, and W. Menzel, "Novel dual mode substrate integrated waveguide band-pass filters," *J. Electromagn. Waves and Appl.*, Vol. 24, No. 11–12, 1661–1672, 2010.
24. Chen, T., "Determination of the capacitance, inductance, and characteristic impedance of rectangular lines," *IEEE Trans. Microw. Theory Tech.*, Vol. 8, No. 5, 510–519, 1960.
25. CST Microwave Studio®, CST Computer Simulation Tech. AG.
26. Shin, J. and D. Schaubert, "A parameter study of stripline-fed Vivaldi notch-antenna arrays," *IEEE Trans. Antennas Propag.*, Vol. 47, No. 5, 879–886, 1999.
27. Agilent ADS®, Agilent Technologies Inc.